J Mater Sci (2012) 47:649–658
DOI 10.1007/s10853-011-5835-7

A tribological and biomimetic study of PI–CNT composites for cartilage replacement

R. Ribeiro · S. Banda · Z. Ounaies · H. Ucisik · M. Usta · H. Liang

Received: 5 February 2011 / Accepted: 29 July 2011 / Published online: 11 August 2011

Abstract This article presents an investigation into the possible matching of mechanical properties of a polyimide (PI)–carbon nanotube (CNT) composite system to natural cartilage tissue. Currently used ultrahigh molecular weight polyethylene (UHMWPE) used in total joint replacements presents certain drawbacks due to a mismatch in mechanical and tribological properties with those of a natural bone joint. Natural cartilage tissue is a composite material itself, being composed of collagen fibers, hydrophilic proteoglycan molecules, cells and other constituents. The current investigation attempts to mimic the mechanical and tribological properties of natural cartilage tissue by varying the CNT concentration in a PI matrix. Nanoindentation and pin-on-flat tribological tests were conducted for this purpose. It was found that the coefficient of friction (COF) reached a minimum at a concentration of 0.5% CNT (by volume) when articulated against Ti6Al4V alloy. When articulated against Ti6Al4V alloy in the presence of a lubricant, the minimum COF was obtained at a concentration of 0.2% CNT. The maximum penetration depth under nanoindentation varied with CNT concentration and indicated that the mechanical properties could be tailored to match that of cartilage tissue. A closer investigation into this behavior was carried out using scanning electron, transmission electron, and atomic force microscopy. It was noticed that there is good bonding between the CNTs and polyimide matrix. There was a ductile to brittle transition as the concentration of CNT was increased. Competing interactions between nanotube–matrix and nanotube–nanotube are possible reasons for the deformation and friction behavior identified.

R. Ribeiro · H. Liang (✉)
Department of Mechanical Engineering, Texas A&M University, College Station, TX 77843, USA
e-mail: hliang@tamu.edu

R. Ribeiro · Z. Ounaies · H. Liang
Materials Science and Engineering, Texas A&M University, College Station, TX 77843, USA

Present Address:
R. Ribeiro
Department of Mechanical Engineering, Indian Institute of Technology Delhi, Hauz Khas, New Delhi 110016, India

S. Banda · Z. Ounaies
Department of Aerospace Engineering, Texas A&M University, College Station, TX 77843, USA

H. Ucisik
Department of Prostheses, Materials and Artificial Organs, Institute of Biomedical Engineering, Bogazici University, 80815 Bebek, Istanbul, Turkey

M. Usta
Department of Materials Science and Engineering, Gebze Institute of Technology, 41400 Gebze, Kocaeli, Turkey

Introduction

To date, the most popular method of treatment of severe arthritis is total joint replacement (TJR). This technique is irreversible, and requires a substantial amount of surgery. It does not provide a very natural form of recovery, and the prostheses do not last more than 10–15 years, on average [1, 2]. Problems encountered are prostheses loosening, wear of articulating surfaces, and inciting of a negative immune response, leading to necrosis. Some of the reasons for failure are micro-motion at the bone–implant interface caused by differing mechanical properties, lack of

biocompatibility, and inadequate fixation of the implant. Another problem encountered due to mismatch in mechanical properties between tissue and the prostheses is stress shielding. This is a phenomena in which the prosthetic implants, having a higher modulus than the tissue, takes on higher loads causing the surrounding bone to bear lower loads than usual. This causes disruption of the normal bone remodeling process leading to decreased bone tissue. A desired characteristic in joint prostheses is the ultralow coefficient of friction ($\sim$0.01) found in natural joints. Therefore, in order to overcome the drawbacks of TJR and reduce the need for subsequent surgeries, the goal is to produce materials that match the mechanical and tribological properties of bone and cartilage tissue, are more biocompatible, and form a better interface between the bone and the implant.

Ultrahigh molecular weight polyethylene (UHMWPE) is one of the most popular polymers used in joint arthroplasty due to its low friction, high impact strength, excellent toughness, low density, ease of fabrication, biocompatibility, and biostability [1]. The wear debris that comes off the surface of this material is, however, the main cause for joint replacement failure, due to the negative immune response that is incited [1]. UHMWPE has unique properties related to its microstructure. It has been reported that heating UHMWPE to temperatures even below its melting point can significantly alter its crystallinity and physical properties [3]. In addition, resistance to crack propagation improves when the crystallinity increases [4]. Radiation sterilization, in the presence of air can lead to chain scission, decrease in molecular weight, increased crystallinity, oxidation, accompanied by decreased mechanical strength [5]. Crosslinking the polymer enhances the resistance to plastic flow and lamellae alignment at the articulating surface, resulting in better resistance to wear [6, 7]. However, there is a tradeoff with decreased mechanical properties that include strength, ductility, elastic modulus, fracture toughness, and crack propagation resistance [8]. In UHMWPE tibial inserts, the components are subjected to high cyclic contact stresses. This results in pitting and delamination [9]. It has also been found that large-scale deformation and plasticity induced damage layers develop under the articulating surface due to sliding and high contact stresses [10].

Polyimides have been widely used in the fabrication of aircraft structures and microelectronic devices [11]. They perform well under high temperatures, radiation and heavy mechanical loads [12]. In addition they also exhibit high wear resistance, low friction, high strength and toughness, and dimensional stability [12]. Richardson et al. [13] reported that polyimides exhibited no cytotoxic response and little hemolysis. Moreover, polyimides adsorbed large amounts of body serum albumin (BSA) and fribrinogen. They also showed excellent film forming ability, electrical properties, and sterilizability. Cai et al. [14] reported that PI/CNT nanocomposites exhibited lower friction than pristine PI. Carbon nanotube (CNT) as a reinforcing agent also contributed to restrain the adhesion and scuffing of the PI matrix. These reports indicate promise that PI/CNT composites could replace UHMWPE as a joint replacement material.

A CNT is essentially a rolled-up grapheme sheet with capped ends. The cylindrical diameter is in the range of 0.4–2 nm [15]. A single-walled carbon nanotube (SWNT) is made up of a single cylindrical graphite sheet, whereas a multi-walled carbon nanotube (MWNT) is made up of concentric cylinders of graphite. CNTs possess high tensile strength, ultra-light weight and have excellent thermal and chemical stability [11]. Carbon-based materials have been widely used as biomaterials [16–18]. CNTs are therefore a potential candidate for use as a multifunctional material in biomaterial composites. The mechanical strength can provide reinforcement similar to collagen fibers and functionalization of the CNT surface can tune the attractive and reactive forces within and on the surface of the composite materials. Over the past decade, great strides have been made in exploiting the unique combination of properties of CNTs [19–22] through polymer nanocomposite processing. It follows that a key issue in CNT–polymer composites is how to tune the CNT–polymer interface to take advantage of the electronic and mechanical properties of CNTs. Both surface and bulk measurements can provide important information on the CNT–polymer and CNT–CNT interaction mechanisms.

Buldum and Lu [23] have investigated the sliding of nanotubes and measured the friction force associated with stick slip motion of nanotubes using atomic force microscopy. An increase in the loss factor of epoxy was seen by the addition of SWNTs and MWNTs [24, 25]. The nanoscale dimensions and high aspect ratio of nanotubes result in a large interfacial contact area. The high interfacial contact area can result in high frictional energy dissipation during the sliding of nanotube surfaces within the composite. There are two possible mechanisms that have been reported, frictional sliding at the nanotube–nanotube and nanotube–matrix interface [26, 27].

Suhr et al. [26] reported an increase in mechanical damping in epoxy polymer composites due to the presence of CNTs. There was a 15-fold increase in damping compared to the pure epoxy. Estimating the critical shear stress for the onset of slip at the nanotube–polymer interface it is reported that there is no possibility for tube–polymer slip in this system [26]. The tube–tube slip in the system is activated at low strains as the shear stress for tube–tube sliding is estimated to be low. As the strain increases there are more number of sites that are activated, resulting in an

increase in damping. Damping is related to frictional energy dissipation during interfacial sliding at the long spatially distributed CNT–CNT interfaces. Simulation studies by Yakobson et al. [28] indicated that CNTs are extremely resilient, and can sustain extreme strain with no signs of brittleness, plasticity, or atomic rearrangements. Experiments by Barber et al. [29] indicated that the polymer matrix around the nanotube was able to withstand high levels of stress that would otherwise see a similar bulk polymer sample fail.

A similar increase in damping was seen for SWNT–PC composite. The damping behavior in this system is driven by tube–matrix slip. A composite with better dispersion showed greater damping compared to the poorly dispersed case. Better dispersion reduces the nanotube clusters and improves the polymer nanotube interaction. If the system undergoes a tube–tube slip mechanism, it is expected that bad dispersion leads to a decrease in damping. It is reported that the interaction between the polymer and nanotube results in the increase [25].

The low friction properties of graphite are well known due to its lamellar crystal structure [30, 31]. It was reported by Cai et al. [14] that PI–CNT composites exhibited lower coefficient of friction and lower wear than neat PI under dry sliding. The percentage of CNT by weight ranged from 0 to 30%. However, there was no investigation of the composites with a CNT concentration between 0 and 2 wt%. Vander Wal et al. [32] investigated the tribological effects of fluorinating the surfaces of CNTs. They reported coefficients of friction in the range 0.002–0.07 indicating that surface modified nanocarbons can be used as solid lubricants. Atomistic simulation studies of nanotubes by Ni and Sinott [33] indicated that nanotubes are flexible in the direction perpendicular to the axis and stiff in the direction of the axis. It was found that at high compressive pressures, the vertically arranged nanotubes are able to buckle whereas the horizontally arranged tubes plastically deform. Park et al. [34] reported effective wetting of nanotube surfaces by a polyimide matrix, using electron energy loss spectroscopy.

The current research investigates the surface and bulk characteristics of a PI/CNT composite with varying CNT concentrations and also compares its tribological and mechanical characteristics with natural cartilage and joint replacement materials. The composite system is based on a good dispersion between unfunctionalized SWNTs and a dipolar polymer, where no surfactant was used. The dispersion is believed to result from a good noncovalent interaction between the SWNTs and the polymer. The series of bulk and surface techniques highlight the interaction mechanism present and inform on the dispersion and interaction mechanism as a function of SWNT content.

Materials

Polyimide

Polyimide was synthesized by reacting 2,6-bis-(3-amino phenoxybenzo nitrile) (βCN-APB) with 4,4-oxydiphthalic anhydride (ODPA). They were initially dissolved in a solvent *N*,*N*-dimethylacetamide (DMAC). The product formed was polyamic acid. On heating, water was liberated from the polyamic acid, forming the polyimide product.

Carbon nanotubes

Hipco processed SWNTs were obtained from Carbon Nanotechnologies Inc. The details on the polymerization and composite preparation can be found in Ref. [35]. Polyimide was combined with SWNTs, during the polymerization stage. Samples were prepared with different nanotube concentrations (0.035, 0.05, 0.075, 0.1, 0.2, 0.5, 1, 2, and 5 vol.%). Details on processing are discussed in earlier publications [36, 37].

Ultrahigh molecular weight polyethylene

Ultrahigh molecular weight polyethylene (UHMWPE) was obtained from Goodfellow Inc., in processed form. It is a semi-crystalline, whitish, and effectively opaque engineering thermoplastic which, chemically, has a very high molecular weight (3–6 million) [38]. As a result it has an extremely high (effectively infinite) melt viscosity and can only be processed by powder sintering methods. It also has outstanding toughness, cut and wear resistance and very good chemical resistance. Specimens were cut into rectangular plates approximately 10 mm (length) $\times$ 10 mm (width) $\times$ 2 mm (height). It was used as a control material to compare properties with the polyimide nanocomposites.

Titanium alloy

The Titanium alloy 90Ti6Al4V has been widely used in bone joint tribological applications. We therefore used this material as a counter material against the PI–CNT composite for the tribo-tests. Ti6Al4V alloy was obtained from Goodfellow Inc. The specimens were cut into cylinders of 10 mm diameter and approximately 8 cm. height. They were used as the pin in the tribo tests, with the cylinder base as the articulating surface.

Articular cartilage

Human articular cartilage specimens were obtained from a 51-year-old male's amputated right knee. The patient was suffering from a vascular obstructive disease in his right

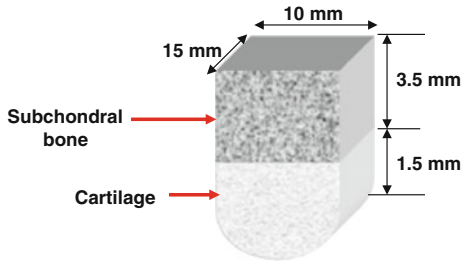

Fig. 1 Approximate dimensions of cartilage and subchondral bone specimen

leg. He had no chance of living with conservative treatment because of ischemic necrosis of the foot. Therefore, his leg had to be amputated above the knee. The specimens were harvested from the amputated joint using a hacksaw and scalpel blade. The specimens contained the entire thickness of cartilage and part of the subchondral bone (Fig. 1). Cartilage and subchondral bone obtained from near the femoral condyle was used as the pin material in the tribological tests. Cartilage (complete thickness) and subchondral bone from the tibial plateau was used as the counter material for the cartilage–cartilage tests. Subchondral bone from the knee joint of the same subject from whom the cartilage was obtained, was used in these studies. The bone and cartilage specimens were stored in a frozen condition at −17 °C. Before testing, cartilage/bone specimens were hydrated to the maximum limit by immersing in water for approximately 10 min.

Simulated synovial fluid

Initially, a solution of simulated body fluid (SBF) was prepared. The ionic composition of SBF is given in Table 1. This liquid solution was originally prepared by Kokubo et al. [39].

The concentration of hyaluronic acid in synovial fluid has been reported as 0.1–5 mg/mL [40]. Based on this, a concentration of 3 mg of hyaluronic acid (Rexall Inc., Boca Raton, FL) was added per mL of SBF. The mixture was then sonicated for 10 min to disperse the hyaluronic acid particles in the fluid. The resulting fluid was stored in a refrigerator at 3 °C. This solution was applied between the articulating surfaces before the tests were started.

Table 1 Ionic concentrations present in SBF

Ion	Concentration (mM)
Na^+	142.0
K^+	5.0
Mg^{2+}	1.5
Ca^{2+}	2.5
Cl^-	147.8
HCO^{3-}	4.2
HPO^{4-}	1.0
SO_4^{2-}	0.5

Experimental methods

Friction tests

A CSM Instruments tribometer was used in the pin-on-flat configuration, for the tribo-tests. The temperature at the interface was maintained at body temperature (37 °C), using a heater attached to the reciprocating stage. The motion was linear reciprocating with an amplitude of 3 mm and the speed of movement was 1.5 cm/s, in an attempt to simulate natural joint motion. The coefficient of friction against the number of cycles and time was plotted using TriboX software (CSM Instruments), as the experiments progressed.

Nanoindentation

Nanoindentation tests were conducted using a Hysitron triboindenter. The indenter tip used was of a Berkovich type. The loading–unloading curve is shown in Fig. 2. The loading condition was an initial linear increase from 0 to 200 μN in 10 s, followed by a stable load of 200 μN for 10 s, finally followed by a linear decrease in load from 200 to 0 μN over 10 s. The indenter moved in a direction perpendicular to the sample surface. Software supplied by Hysitron was used to determine the load–depth profile. Figure 3 shows the profile of the nano-triboindenter tip. The radius of the nanoindenter tip was 150 nm.

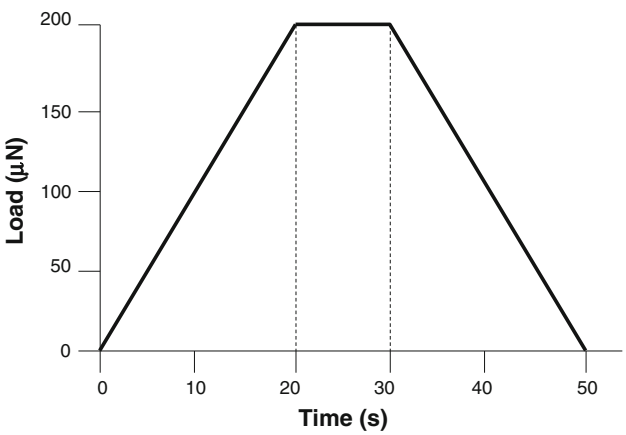

Fig. 2 Loading–unloading curve for the nanoindentation tests

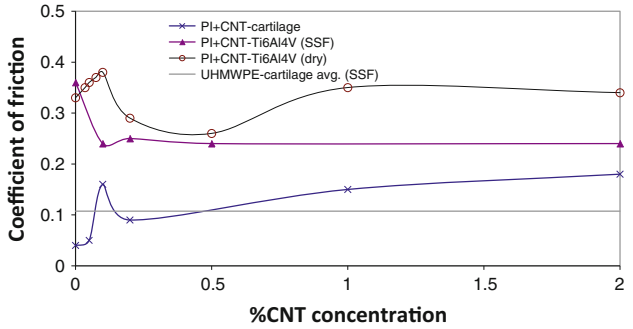

Fig. 3 Comparison of friction coefficient as a function of CNT content for various sample configurations. Value for UHMWPE–cartilage has been included for comparison

Scanning electron microscopy

For SEM imaging, first both surface and fracture surface of the films were coated by a plasma sputter-coater using a platinum target and then samples were imaged by a FE-SEM (FEI Quanta 600). To obtain the fracture surface samples, the nanocomposites were initially frozen in liquid nitrogen after introducing a small notch on the sample.

Transmission electron microscopy

Images of wear particles obtained from the friction tests were obtained with a transmission electron microscope (TEM, JEOL 2010). The operating voltage was 200 kV and the source was made of LaB_6. Samples for testing were collected in the form of wear particles from the specimen wear tracks after the tribo-tests. The particles were mixed in acetone and dispersed by placing the solution in a sonicator for 10 min. A drop of this solution was then applied onto a 400 mesh copper, carbon stabilized, formvar TEM test grid. The acetone was allowed to evaporate, leaving behind the debris.

Atomic force microscopy

An atomic force microscope (Pacific Nanotechnologies Inc.) was used to obtain topography and phase images in close contact mode. Images were obtained from the wear tracks after the wear tests were conducted.

Dynamic mechanical analysis

A dynamic mechanical analysis (DMA) of the films was done using a dynamic mechanical thermal analyzer (RSA-III, TA Instrument). Samples were cut from films in 50×5 mm^2 planar dimensions. Measurements were done in 1 Hz frequency between -100 to 150 °C at a rate of 3 °C/min, in tension mode. During the tests, the sample was subjected to a constant load. The applied stress was in the form of a sinusoidal signal, such that the strain on the sample would be sinusoidal. If a sample is perfectly elastic, both stress and strain will be in phase, otherwise there will be a phase and time lag between them. The DMA test is always conducted in the linear viscoelastic range. In DMA, a complex modulus (E^*), storage modulus (E'), and imaginary loss modulus (E") are calculated from the material response to the sine wave. The complex modulus is defined by $E^* = E' + iE''$ where E' is the real part of the modulus, which is a measure of stiffness, E'' is the imaginary part of the modulus, which is a damping or energy dissipation factor and $i = \sqrt{-1}$. The angle that reflects the time lag between the applied stress and measured strain is δ, and it is defined as:

$$\tan \delta = \frac{E''}{E'} \tag{1}$$

Tan δ, a damping term, is a measure of the ratio of energy dissipated as heat to the maximum energy stored in the material during one cycle of oscillation. The main peak exhibited by tan δ is the primary relaxation or α peak. The temperature at which the intensity of the α peak is maximum corresponds to the glass transition temperature (T_g).

Results

Friction

Figure 3 illustrates plots of the coefficient of friction against %CNT for the PI–CNT composites, under three different lubrication conditions—when articulated against cartilage with SSF between the surfaces, when articulated against Ti6Al4V under dry conditions, and when articulated against Ti6Al4V with SSF between the surfaces. For comparison, the average coefficient of friction measured when UHMWPE is worn against cartilage is superimposed. For the dry condition, at a %CNT concentration of approximately 0.5, there is a minimum in the coefficient of friction. The coefficient of friction ranges approximately between 0.24 (0.5% CNT) and 0.44 (0.075% CNT). These values of coefficient of friction are much higher than the values found in natural joints ($\sim$0.01). However, there is definite evidence that at an optimum concentration of CNTs, the coefficient of friction can be minimized. We can see that the COF of the PI composite against Ti6Al4V under dry conditions is the highest. The presence of SSF between the surfaces caused a lowering in the COF at all NT concentrations. The lowest COF values are, however, noticed for the PI composite when tested against cartilage. The average COF ($\sim$0.11) for UHMWPE against cartilage

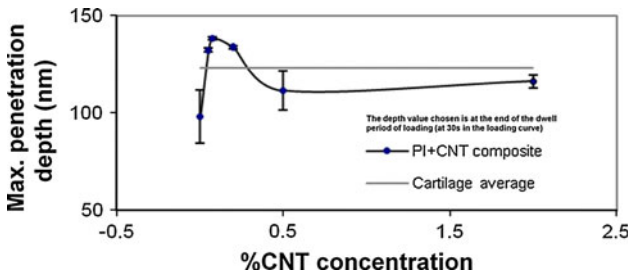

Fig. 4 Maximum penetration depth versus %CNT for the PI–CNT composites with average maximum penetration depth for cartilage superimposed

is found to lie in between the values found for different concentrations of CNT within the PI matrix.

Nanoindentation

Figure 4 shows the variation in the maximum penetration depth of the PI–CNT composite as a function of CNT concentration, during the nanoindentation tests. On this, is superimposed, the average value of maximum indentation depth for natural cartilage tissue. It can be seen that, in the composite, there is greatest deformation at a CNT concentration of 0.05% followed by a decrease up to a CNT concentration of 0.5%, and thereafter stabilizes. The maximum deformation for cartilage tissue lies in-between that for 0.035% CNT and pristine PI samples, and in-between that for 0.2 and 0.5% CNT. This indicates a possible tailorability of the PI–CNT composite to bring it to match the mechanical behavior of natural cartilage tissue.

Scanning electron microscopy

Figure 5a and b is the image of the worn surface of the PI + 2% CNT composite. It is evident that the nanotubes tend to remain embedded in the matrix with a sheath of matrix attached to the protruding portion of the nanotubes. This indicates good bonding between the nanotube and matrix.

Transmission electron microscopy

Figure 6a and b are the TEM images of CNTs embedded within the PI matrix. These are images of wear particles that came off the composite surface with 2% CNT, during the friction tests. There is indication that the particles were torn off around the CNTs, indicating that the CNTs adhere

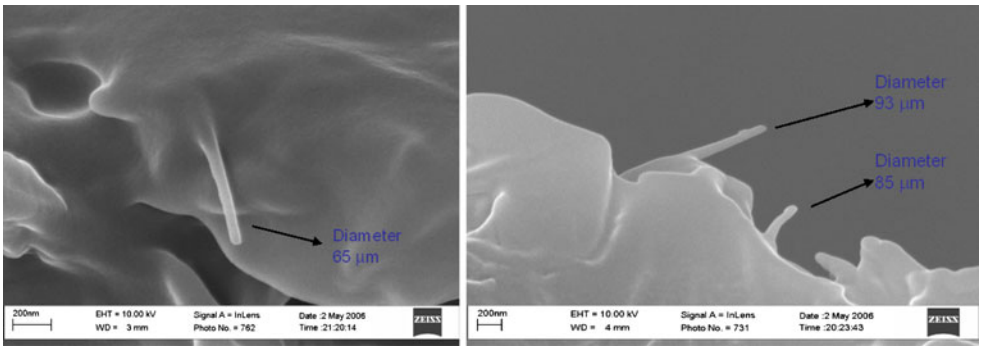

Fig. 5 SEM of PI + CNT worn surface showing nanotubes protruding, covered with a sheath of PI matrix

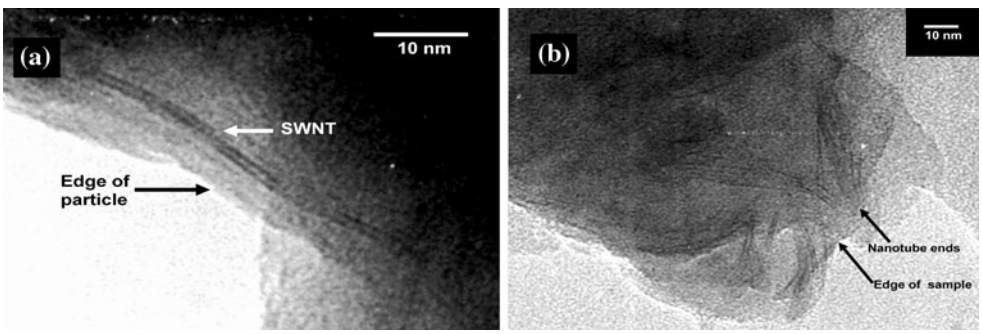

Fig. 6 TEM of a worn particle of PI + CNT showing that the particle tore around the nanotubes, which act as crack arrestors

well to the PI matrix. This is an indication of the strong bonding between the CNTs and PI.

Atomic force microscopy

Figure 7a–d shows the AFM topography (on the left) and phase (on the right) images of the wear tracks of pure PI, PI + 0.1% CNT, PI + 0.5% CNT, and PI + 2% CNT when worn against Ti6Al4V alloy under dry conditions. This information was necessary to determine the internal and surface structure of the composite with change in nanotube concentration. Figure 7a–d indicates that the nature of wear changes as the concentration of nanotubes increases. The wear track of pristine polyimide has regular abrasive wear grooves (Fig. 7a). The phase image indicates a fairly uniform phase throughout. Figure 7b shows abrasive wear grooves in the direction of sliding, as well as striations perpendicular to the sliding direction for the case of PI + 0.1% CNT. The surface of the wear track for PI + 0.5% CNT (Fig. 7c) indicates large pores on the wear track. Finally, the wear track of the sample with 2% CNT shows crystalline grains with inter-granular like cracks (Fig. 7d). This indicates a somewhat ductile to brittle transition with increase in nanotube concentration.

Dynamic mechanical analysis

In Fig. 8, it is seen that there was an increase in the damping behavior of CNT–polyimide composite up to 0.1 vol% CNT, and then there was a decrease in damping at higher CNT concentrations.

Discussion

It is noticed in Fig. 4 that the friction coefficient increases from an SWNT concentration of 0–0.1% and thereafter decreases, during the dry tests against Ti6Al4V. This peak in friction coefficient corresponds with a peak in tan δ value as shown in Fig. 8 (indicating maximum damping) at 0.1% SWNT. The nanoindentation curves (Fig. 5) indicate maximum deformation within the range of 0.05–0.2% SWNT. The deformability causes larger surface contact between surfaces leading to higher friction. The worn surface image for an SWNT concentration of 0.1% (Fig. 7b) shows ripples on the surface in a direction perpendicular to the direction of sliding. These ripples are caused by the softness of the surface. The friction coefficient under dry conditions is minimum at 0.5% SWNT which corresponds with high stiffness indicated by a low tan δ value as well as a lower indentation depth in Fig. 5. The corresponding AFM image (Fig. 7c) indicates a pore-like surface. This could be due to the higher clustering of nanotubes, causing them to agglomerate and separate from the surface, leaving behind the pore spaces. At a maximum SWNT loading of 2%, the COF increases to a value of approximately 0.34 (Fig. 4). This corresponds with higher stiffness indicated in Fig. 5 (nanoindentation) and Fig. 8 (tan δ). The corresponding AFM images (Fig. 7d) show a highly crystalline-like worn surface with inter-granular cracks. SEM (Fig. 5) and TEM (Fig. 6) images indicate that the nanotubes remain well bonded to the matrix and particles tend to tear off the surface around the nanotube clusters.

The inclusion of a lubricant between the surfaces tends to decrease the COF when CNTs are included in the matrix (Fig. 4). In the case of pristine PI, the COF is not affected by the presence of SSF. With CNT loading, the COF drops to a value of approximately 0.23 and is not greatly affected with different concentrations of CNT. There is a possible interaction between the SSF molecules and the nanotubes. This needs to be investigated further. As expected, when the PI–CNT composite is articulated against cartilage, the COF is much lower as compared with Ti6Al4V. The curve for PI–CNT against cartilage is similar to the curve for PI–CNT against Ti6Al4V under dry condition. There is a maximum COF around 0.1% CNT. The COF then drops and increases further, indicating that there is an optimum SWNT concentration at which a minimum COF can be obtained. The average COF value for UHMWPE when worn against cartilage lies in-between values obtained with the PI–CNT against cartilage, indicating an improvement in the COF as compared with UHMWPE.

The coefficient of friction ranges approximately between 0.24 (0.5% SWNT) and 0.44 (0.075% SWNT). These values of coefficient of friction are much higher than the values found in natural joints ($\sim$0.01). However, there is definite evidence that at an optimum concentration of CNTs, the coefficient of friction can be minimized. We can see that the COF of the PI composite against Ti6Al4V under dry conditions is the highest. The presence of SSF between the surfaces caused a lowering in the COF. The lowest COF values are however noticed for the PI composite when tested against cartilage.

From the above discussion, we can conclude that at a %CNT concentration in the range 0.2–0.5 wt%, PI–CNT composites have a unique behavior. Overall, there is a transition from a harder but ‘not very brittle’ surface character at lower concentrations, to a soft, highly deformable character at 0.2 to 0.5% CNT, followed by a hard and brittle character at higher concentrations. The effects of nanotubes lie not only in strengthening the polymer, but also in their mutual surface interactions and deformability. Interactions between nanotubes are of two forms, as shown in Fig. 9a and b. Undeformed nanotubes

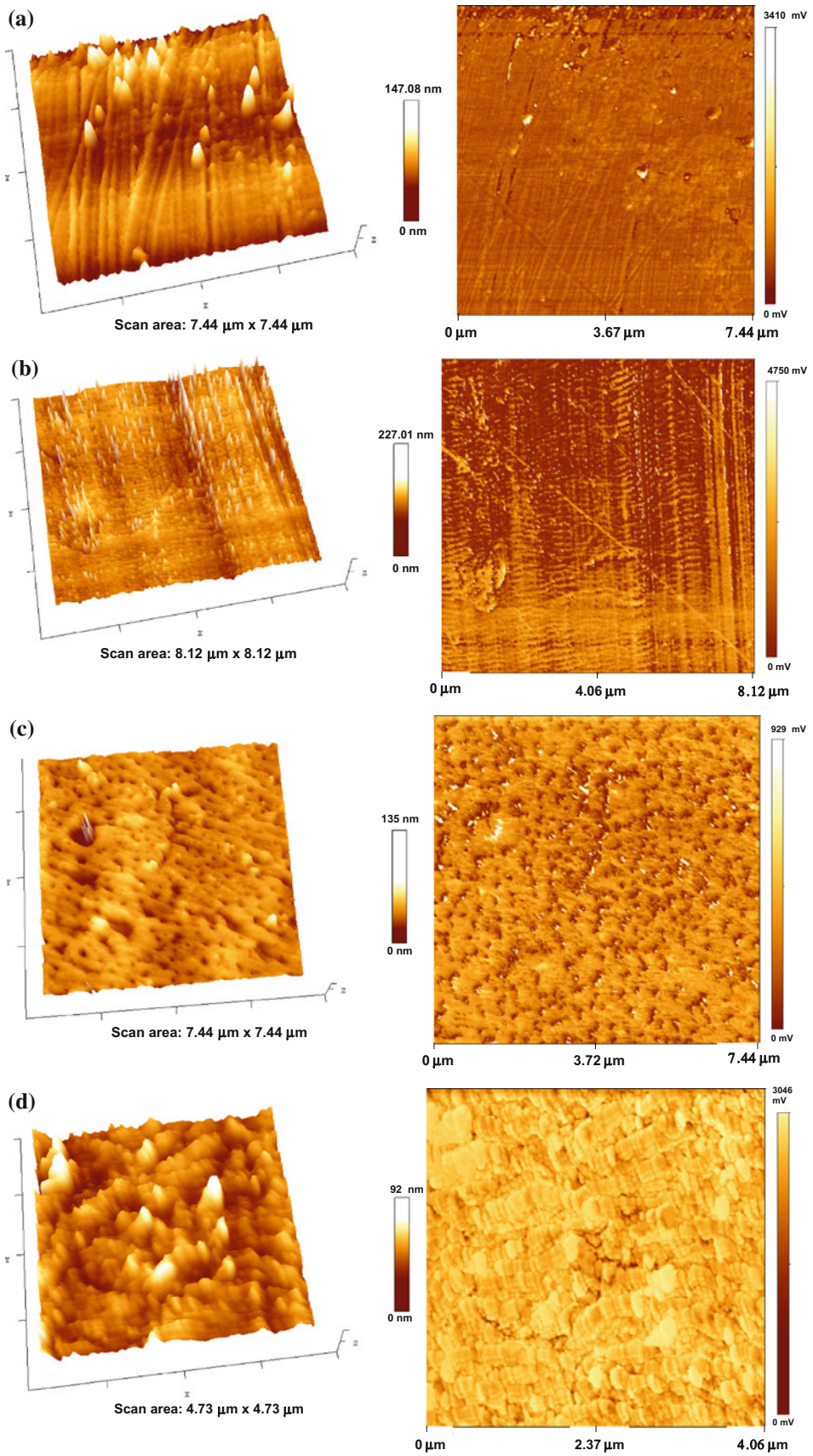

Fig. 7 AFM topography (*left*) and phase (*right*) images of the worn surfaces of PI + CNT composite: **a** Pristine PI, **b** PI + 0.1% CNT, **c** PI + 0.5% CNT, **d** PI + 2% CNT

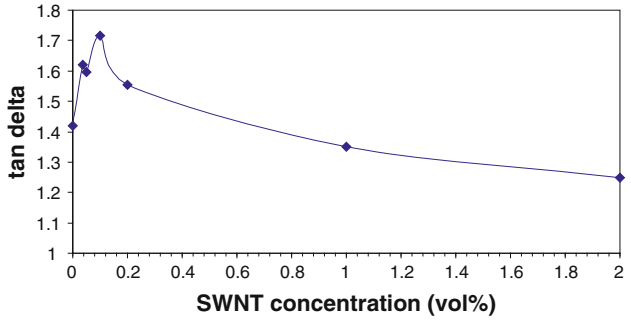

Fig. 8 DMA tan δ versus CNT concentration indicating an increase in damping up to a loading of 0.1% CNT followed by a gradual decrease

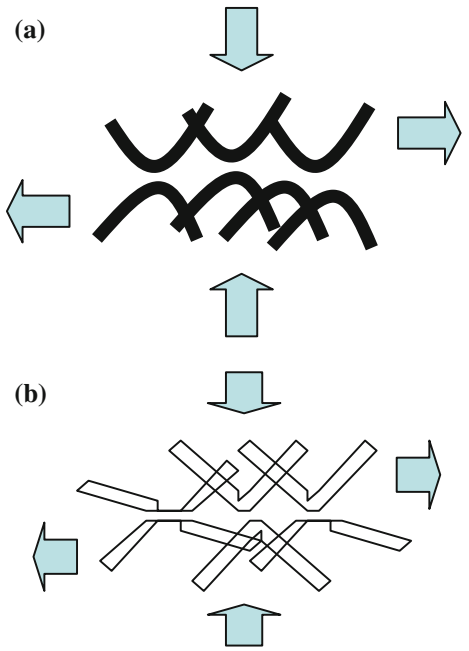

Fig. 9 Interfacial sliding of **a** undeformed nanotubes and **b** deformed nanotubes

can absorb the impacts of loads and also slide against each other (as there is no chemical bond between adjacent nanotubes). At higher nanotube concentrations, the surface tends to be more crystalline due to the orientation of groups of nanotubes in the same direction. The nanotubes also tend to get compressed to the limit (Fig. 9a) and are not able to absorb applied loads. This leads to high loads on the interacting surfaces and an increase in COF. At low %CNT concentrations, there is insufficient sliding between nanotubes and therefore the COF is high.

These characteristics of nanotube deformability and surface interactions can cause the friction and modulus trend noticed. In the range 0.2–0.5% CNT concentration, there could be high efficiency of sliding and deformability leading to the low values of modulus and COF.

Conclusions

The properties and applications of a polymer nanocomposite enhanced by CNTs in potential bone joint applications was investigated. The PI + CNT composites showed improved performance over UHMWPE. The nanomechanical properties are close to that of cartilage. Altering the concentration of nanotubes resulted in a change in tribological properties. Alignment and functionalization of the nanotubes can lead to tailored properties that could possibly improve in vivo interaction with tissue, enzymes and synovial fluid. The friction and deformation behavior of PI + CNT composite surfaces were found to be associated with three possible interfacial interactions. They are CNT–PI, CNT–CNT, and CNT-deformed CNT interactions.

At low CNT loading the good interfacial interaction leads to a slip between the matrix and the CNTs and simultaneously there is also a tube–tube slip occurring between individual CNTs present in clusters. A combination of tube–tube slip and tube–matrix slip might be the reason for the increase in damping.

As the SWNT concentration is increased there is a large increase in the stiffness of the system, which results in reducing the energy dissipated. Even though there is more tube–tube slip in the system at high CNT concentrations, the stiffness of the matrix impedes the damping behavior.

Two mechanisms: (1) CNT presence results in less friction: localized drag and better adhesion; and (2) polymer chains are stiffer due to the presence of inclusions, and a strong interface between PI and CNTs. Basically, there is adhesion versus stiffness. In one case, adhesion is dominant, in the other, stiffness is dominant.

Acknowledgements The authors acknowledge the financial support of US National Science Foundation (0535578). They also wish to thank the support of the Materials Characterization Facility and the Microscopy Imaging Center at the Texas A&M University for surface characterization.

References

1. Lewis G (1997) J Biomed Mater Res 38(1):55
2. Sargeant A, Goswami T (2006) Mater Des 27(4):287
3. Li S, Burnstein AH (1994) J Bone Joint Surg 76A:1080
4. Gómez-Barrena E, Chang JD, Li S (1996) In: Pritchard DJ (ed) Instructional course lectures 45. American Academy of Orthopaedic Surgeons, Rosemont, IL
5. Premnath V, Harris WH, Jasty M, Merill EW (1996) Biomaterials 17:1741

6. Edidin AA, Pruitt L, Jewett CW, Crane DJ, Roberts D, Kurtz SM (1999) J Arthroplasty 14(5):616
7. Wang A, Sun DC, Yau SS, Edwards B, Sokol M, Essner A, Polineni VK, Stark C, Dumbleton JH (1997) Wear 203:230
8. Pruitt LA (2005) Biomaterials 26:905
9. Pascaud RS, Evans WT, McCullagh PJ, Fitzpatrick DP (1997) Biomaterials 18:727
10. Kurtz SM, Rimnac CM, Pruitt L, Jewett CW, Goldberg V, Edidin AA (2000) Biomaterials 21:283
11. Jiang X, Bin Y, Matsuo M (2005) Polymer 46:7418
12. Shen C, Dumbleton JH (1976) Wear 40:351
13. Richardson RR, Miller JA, Reichert WM (1976) Biomaterials 14(8):627
14. Cai H, Yan F, Xue Q (2004) Mater Sci Eng A 364:94
15. Smart SK, Cassady AI, Lu GQ, Martin DJ (2006) Carbon 44:1034
16. Cenni E, Granchi D, Arciola CR, Ciapetti G, Savarino L, Stea S (1995) Biomaterials 16(16):1223
17. Ma L, Sines G (1983) J Biomed Mater Res 51A(1):61
18. Haubold AD (1983) ASAIO J 6:88
19. Treacy MMJ, Ebbesen TW, Gibson JM (1996) Nature 381:678
20. Falvo MR, Clary GJ, Taylor RM, Chi V, Brooks FP, Washburn S (1997) Nature 389:582
21. Ebbesen TW, Lezec HJ, Hinura H, Bennett JW, Ghaemi HF, Thio T (1996) Nature 382:54
22. Dai H (2002) Acc Chem Res 35:1035
23. Buldum A, Lu JP (1999) Phys Rev Lett 83:5050
24. Zhou X, Shin E, Wang KW, Bakis CE (2004) Comp Sci Technol 64(15):2425
25. Koratkar N, Suhr J, Joshi A, Kane R, Schadler L, Ajayan P, Bartolucci S (2005) Appl Phys Lett 87(6):063102
26. Suhr J, Koratkar N, Keblinski P, Ajayan P (2005) Nat Mater 4:134
27. Koratkar N, Wei BQ, Ajayan PM (2002) Adv Mater 14:997
28. Yakobson BI, Brabec CJ, Bernholc J (1996) Phys Rev Lett 76(14):2511
29. Barber AH, Cohen SR, Wagner DH (2003) Appl Phys Lett 82(23):4140
30. Savage RH (1991) J Appl Phys 19(1):1
31. Mangalick MC (1974) Carbon 12(5):573
32. Vander Wal RL, Miyoshi K, Street KW, Tomasek AJ, Peng H, Liu Y, Margrave JL, Khabashesku VN (2005) Wear 259:738
33. Ni B, Sinott SB (2001) Surf Sci 487:87
34. Park C, Crooks RE, Siochi EJ, Harrison JS, Evans N, Kenik E (2003) Nanotechnology 14:L11
35. Banda S (2004) Characterization of aligned carbon nanotubes/polymer composites. MSc thesis, Virginia Commonwealth University, Richmond, VA
36. Deshmukh S, Ounaies Z (2009) Sens Actuators A Phys 155:246
37. Ounaies Z, Park C, Lillehei P, Harrison J (2008) J Therm Comp Mater 21:393
38. Goodfellow Corporation (2010) Oakdale, PA. http://www.goodfellow.com. Accessed 15 August, 2010
39. Kokubo T, Kushitani H, Sakka S (1990) J Biomed Mater Res 24:721
40. Mow VC, Ratcliffe A, Poole AR (1992) Biomaterials 13(2):67